



Spatio-Temporally Weighted Two-Step Method for Retrieving Seismic MBT Anomaly: May 2008 Wenchuan Earthquake Sequence Being a Case

Yuan Qi , Lixin Wu, *Senior Member, IEEE*, Miao He, and Wenfei Mao 

Abstract—Referring to the first law of geography and its extension in time domain, this research makes improvements on the two-step method (TSM) presented to retrieve seismic microwave brightness temperature (MBT) anomaly, and a new method named spatio-temporally weighted TSM (STW-TSM) is developed. Temporally weighted background is calculated using nonseismic data according to respective time intervals with the shocking year, and applied to remove long-term trend so as to retrieve basic MBT residuals. Spatially weighted background is calculated referring to Euclidean geospatial distance away from the epicenter, and applied to eliminate local meteorological noise so as to retrieve cleaned MBT residuals. With May 2008 Wenchuan earthquake sequence being a case study, significant seismic MBT anomalies at H and V polarizations, 10 days before and after the May 12 Mw7.9 main shock, were retrieved using STW-TSM at 6.9, 10.7, 18.7, and 36.5 GHz, respectively. This study shows that the newly developed STW-TSM is much more qualified. More significant seismic MBT anomalies at H polarization was retrieved as compared to V polarization. More detailed and localized MBT anomalies was uncovered from high frequency bands at 18.7 and 36.5 GHz, while much remarkable anomalies (but less details) were obtained from low frequency bands at 6.9 and 10.7 GHz. This research is valuable for satellite MBT observation, seismic anomaly analysis, and earthquake precursor study.

Index Terms—Advanced Microwave Scanning Radiometer for the Earth Observing System, microwave brightness temperature (MBT), seismic anomaly, spatio-temporally weighted, two-step method (TSM).

I. INTRODUCTION

EARTHQUAKE is one of the major natural disasters, whose the monitoring as well as forecasting is of great challenge. However, the satellite remote sensing is providing unprecedented opportunity to monitor seismic activity of planet Earth,

which is capable of detecting seismic-related signals with potential precursory meanings. Since Gorny [1] first applied satellite thermal infrared (TIR) remote sensing data to study the tectonic activity of middle Asia and discovered thermal anomalies before some medium-to-strong earthquakes in 1980's, numerous case studies have confirmed the correlation between apparent anomalous TIR and impending earthquake activities [2]–[14]. However, TIR anomaly of the Earth surface detected by satellite sensors are faint signals and are disabled when thick clouds exist. Therefore, with the aim of detecting and recognizing thermal anomalies related to seismic activities, only cloudless pixels from polar orbit satellite [15], [16] and high frequency data from geostationary sensors that inhibit cloud effects [4], [17] can be adopted and analyzed. With the launching of microwave satellites, microwave remote sensing came into use for retrieving seismic anomalies in recent years [18]–[26] for its continuous and effective data observation.

Phenomena about satellitic microwave radiation anomaly associated with some great earthquakes have been frequently reported since 2008. By using microwave brightness temperature (MBT) data of dual polarizations (horizontal and vertical, in brief H and V) at 18.7 GHz from the Advanced Microwave Scanning Radiometer for the Earth Observing System (AMSR-E) instrument, Maeda and Takano [18] proposed an algorithm for calculating anomaly index based on MBT difference between adjacent pixels after data reconstruction, and applied the presented algorithm to monitor MBT anomaly, near the epicenters of Morocco and Wenchuan earthquakes, that occurred on February 24, 2004 and May 12, 2008, respectively [19]–[21]. These studies indicated there existed MBT anomaly, specifically emitted at 18.7 GHz around the epicenter several days before the shocks. Based on the algorithm presented, a radiation anomaly index (RAI) was further defined by Chen and Jin [22], and Yushu earthquake which occurred on June 17, 2010, which was studied as a case to detect anomaly signals preceding the shock; obvious spatial correlation between RAI anomaly and tectonic faults was revealed. Meanwhile, MBT data at 23.8 GHz were applied to evaluate the influence of ground surface temperature and atmospheric water vapor on seismic anomaly detection. In addition, by collecting MBT data from AMSR-E in Kamchatka Peninsula from 2003 to 2011, Zhang *et al.* [23] used a four-percentile method to determine RAI and made statistics on the time and location information of MBT anomalies before all medium–strong ($M_w > 5.0$) earthquakes

Manuscript received June 15, 2019; revised December 11, 2019; accepted December 24, 2019. Date of publication January 16, 2020; date of current version February 12, 2020. This work was supported in part by the National Key R&D Program of China under Grant 2018YFC15035, in part by the Key Program of the National Natural Science Foundation of China under Grant 41930108, in part by the Innovation Leading Program of Central South University under Grant 506030101, and in part by the Talents Gathering Program of Hunan Province China under Grant 2018RS3013. (Corresponding author: Lixin Wu.)

Y. Qi, L. Wu, and M. He are with the School of Geoscience and Info-Physics, Central South University, Changsha 410083, China (e-mail: wloveqy@163.com; wulx66@csu.edu.cn; 769148060@qq.com).

W. Mao is with the College of Resources and Civil Engineering, Northeastern University, Shenyang 110819, China (e-mail: maowf2014@126.com).

Digital Object Identifier 10.1109/JSTARS.2019.2962719

occurred in Kamchatka over a period of nine years. It was uncovered that most of the earthquakes occurring in Kamchatka, showed identifiable MBT anomalies one month prior the shocks. Singh *et al.* [24] also observed anomalous MBT at 19 and 37 GHz from Special Sensor Microwave/Imager (SSM/I) instrument in ascending and descending modes few days preceding Wenchuan earthquake. Yang and Guo [25] calculated thermal anomalies of Baja California earthquake, occurred on April 4, 2010, using AMSR-E data at 89 GHz, and found that the changing MBT reached its peak 4 days prior to the shock. Recently, Jing *et al.* [26] carried out a detailed analysis on SSM/I MBT data to retrieve thermal anomalies associated with three earthquakes occurred at Tibetan Plateau, and the MBT at 19 GHz indicated higher sensitivity to the seismic anomalies as compared to those at higher frequencies.

However, these reported methods or algorithms focused on only limited and discrete timelines prior to the earthquake, the consecutive spatio-temporal evolution of MBT anomaly during a long seismogenic process were neglected. Besides, the correlation between the regions of abnormal MBT and the seismogenic faults failed to satisfy well with the DTS criterion [27], which was presented as a universal criterion to search for and to make validation of possible earthquake anomalies.

The two-step method (TSM), originally developed by Ma *et al.* [28] in 2011, aims to remove the general effects of background and to eliminate regional meteorological noise in two separate steps so as to retrieve seismic anomaly of satellite MBT. At the first step, the average MBT of multiple years without earthquake is calculated as historical background; at the second step, the average MBT of four corner pixels in a rectangular window is calculated as regional reference field. Then, Liu *et al.* [29], [30] applied this method to retrieve the MBT evolutions of Yushu earthquake and Wenchuan earthquake, and introduced the principle of remote sensing rock mechanics [31] to recognize and explain the occurring of MBT anomalies.

The TSM takes the comprehensive influence of geography, terrain, coversphere, and seasonal factors as a constant for the same day of different years, and the historical data were given the same weights at the first step. And at the second step, weather noises inside the entire study area were considered uniformly distributed without spatial difference. Actually, the impacts of terrain effect [32], coversphere coverage [32], [33], climate change [34], and other long-periodic factors on microwave radiations, will change slowly over time, and the inhomogeneity in similarity will decrease with time and spatial distance. Meanwhile, the short-term variable effects, like meteorological phenomena as wind and rain [35], will alter with terrain and geographic locations and be more relevant between closer sites or pixels, especially within one day.

However, Tobler's first law [36] illustrates that everything is related to everything else, and near things are more related than distant things. In geographic spaces, the geoobjects correspond to locations on the Earth surface with some defined relations between all pairings [37]. Similarly, in the process of seismogenic preparation and shocking, a variety of anomalies might appear within a limited region at different time windows because of crustal stress field altering and a series of coupling

effects [38]–[40]. The abnormal sites or pixels are not absolutely isolated and their presence must be associated with the seismic activity or some tectonic faults, and this correlation should be more obvious in the region closer to seismogenic fault and/or the coming epicenter.

In view of that the additional increments of MBT associated with seismic activities will decrease with distance away from the seismogenic faults or the coming epicenter, and the disturbance from weather and other factors are randomly distributed inside the seismogenic zone, hence the seismic effects on MBT in far-field are thought to be very weak while nonseismic factors are considered to be dominant in the marginal region. Therefore, after the long-term trend being removed at the first step, the basic MBT residuals in periphery are considered to be merely affected by weather disturbance. Possible seismic anomalies would be actually retrieved at the second step if meteorological noise of inner region was successfully eliminated by subtracting a spatial weighting background in consideration of varied geolocation. Furthermore, the space domain of the Tobler's first law was extended to time domain in view of that there also exists "nearness" in time series of historical slices. The temporal weighting reference field for eliminating long periodical effects at the first step can be constructed by using data of different nonearthquake years in light of time intervals away from the shocking year. Hence, the TSM can be improved as spatio-temporally weighted TSM (STW-TSM) by taking the geographical difference and temporal variation [41] into account to construct the historical and regional reference fields of more reliability in the two separate steps.

The disastrous Mw7.9 Wenchuan earthquake, happened in Sichuan Province, China, at 14:28 pm on May 12, 2008 (Beijing Time), and the epicenter located at 31.00°N, 103.32°E, with a depth of 19.0 km. More than 40 aftershocks of magnitude greater than Mw5.0 appeared along the Longmenshan faults after May 12. The seismic mechanism, surface fracturing, and seismic anomalies of the main shock have been frequently studied, while researches on aftershocks are rare. In this article, the Wenchuan earthquake sequence including the main shock was selected for case study to uncover the spatio-temporal evolution of MBT anomalies, and to explore the difference in anomalous MBT between the main shock and aftershocks, so as to compare the capability of proposed STW-TSM with original TSM, and to make a validation on other previous results.

II. METHODOLOGY

As mentioned above, microwave radiation signals from the near-surface of planet Earth and its transmission to satellite sensors are strongly influenced by many factors, including the long-periodic altering effects, like terrain [see Fig. 1(a) and (b)], vegetation coverage and seasonal factors, and short-term capricious effects, like local meteorological conditions. It is widely known that radiation signals received by satellite sensors are actually a mixture of many factors according to the radiative transfer model [42], and the additional increment of seismic signals will be polluted in process of earthquake preparation and shocking. These particular effects in space and time domains are

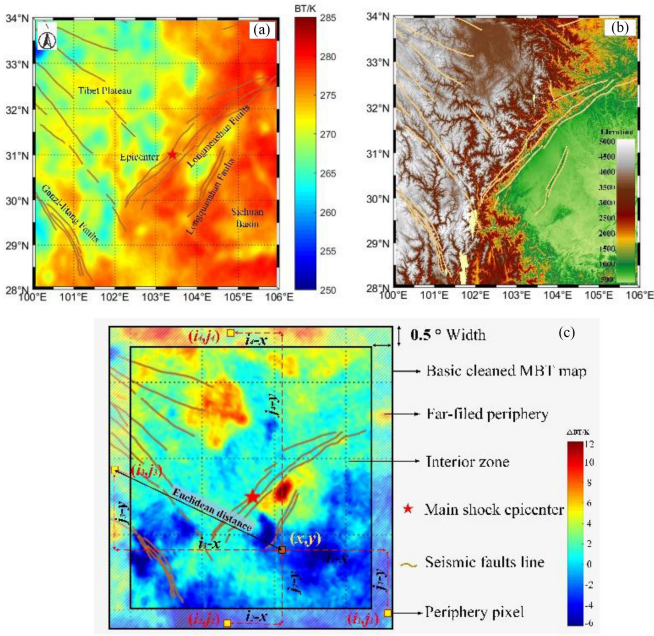


Fig. 1. MBT image someday in any a non-seismic year (a), the terrain of eastern Tibet plateau and western Sichuan basin (b) and the schematic diagram of the second processing step (c). MBT in Sichuan basin is generally higher than that in Tibet plateau, which indicates the general consistency between MBT (a) and elevation (b). Brown interior point (x, y) and the four yellow points (i, j) in periphery (c) represents what needed for the interpolation of a single point, and the whole process goes through every point in respective areas.

primarily incorporated in STW-TSM so as to deal with different pollutions to MBT and to uncover possible MBT anomalies related to seismic activity.

Referring to the first law of geography [36] and its extension in time domain, we endow the historical time slices in different years and adjacent pixels inside the study region with Gaussian function decay-based time weights and space weights, respectively, to effectively eliminate both long-periodical and short-term effects, rather than considering the weights of all historical data the same and the weather effect equally distributed. The STW-TSM is conducted as in the following to obtain the basic and cleaned MBT residuals in two separate steps, respectively.

A. First Step

The first step is to remove the stable and general trend with temporal weighting background as in following equations:

$$W_i = \exp \left[-\frac{(\psi_i - \xi)^2}{D_1^2} \right] \quad (1)$$

$$T_w(x, y, t_\xi) = \frac{\sum_{i=1}^n [W_i \cdot T(x, y, t_i)]}{\sum_{i=1}^n W_i} \quad (2)$$

$$\Delta T(x, y, t_\xi) = T(x, y, t_\xi) - T_w(x, y, t_\xi) \quad (3)$$

where i is the serial number of any nonearthquake year and n is the total years without earthquake happened. ξ represents the earthquake year, ψ_i represents any nonearthquake year with a serial number i , D_1 refers to the maximal year-interval between the shocking year and all nonearthquake years, while W_i is

the temporal weight of MBT data of year i . (x, y) refers to the geographic location of any pixel in the study region, t_ξ is any day in the earthquake year, and t_i represents the same date as t_ξ in any a nonearthquake years. $T(x, y, t_i)$ and $T(x, y, t_\xi)$ stand for the observation values of pixel (x, y) on the date of t_i and t_ξ , respectively. $T_w(x, y, t_\xi)$ is the weighted reference value for the earthquake year calculated from all $T(x, y, t_i)$, $\Delta T(x, y, t_\xi)$ means the basic residual value of pixel (x, y) on the date t_ξ in the earthquake year after the temporally weighted trend being removed.

B. Second Step

Supposing the influence of seismic activity gets reducing with spatial distance away from the epicenter, and after operating at first step, the far-filed periphery of the study region is supposed to be affected only by meteorological factors but not seismic activity. Based on the general-trend-removed basic residual map, the residual values in periphery are used to make inward interpolation pixel-by-pixel according to the Euclidean distance [43] between interior pixel and far-filed periphery pixels [see Fig. 1(c)]. The width of periphery is identified as 0.5° to match the lowest spatial resolution of AMSR-E MBT data (50 km at 6.9 GHz), and ensure that there is at least one valid pixel within this width. The periphery pixel which possesses invalid MBT value, maybe due to the orbit of the satellite instrument, will be neglected during the processing at this step. The spatial weighted MBT residuals of periphery pixels represent possible influence of far-field meteorological disturbance to any interior pixel, and is to be further eliminated from the basic residual map. It works as the following:

$$W_k = \exp \left(-\frac{(i_k - x)^2 + (j_k - y)^2}{D_2^2} \right) \quad (4)$$

$$T_m(x, y, t_\xi) = \frac{\sum_{k=1}^p [W_k \cdot \Delta T(i_k, j_k, t_\xi)]}{\sum_{k=1}^p W_k} \quad (5)$$

$$\Delta \Delta T(x, y, t_\xi) = \Delta T(x, y, t_\xi) - T_m(x, y, t_\xi) \quad (6)$$

where, (x, y) represents the geolocation of any interior pixel and (i_k, j_k) refers to any periphery pixel. D_2 is the diagonal length of the study area, k is the serial number of any periphery pixel, and p is the number of valid pixels in the periphery, W_k refers to the spatial weight of pixel (i_k, j_k) . t_ξ is any day in the earthquake year including the shocking day, $T_m(x, y, t_\xi)$ stands for the interpolated value of far-field meteorological impact on pixel (x, y) in day t_ξ , while $\Delta T(i_k, j_k, t_\xi)$ represents the value of periphery pixel (i_k, j_k) from the differential results of the first step. $\Delta \Delta T(x, y, t_\xi)$ is the cleaned residual value of pixel (x, y) in day t_ξ after eliminating all nonearthquake noises, which represents the possible impacts of seismic activities on MBT.

III. DATA AND PREPROCESSING

As one of the indispensable instruments for Aqua's mission, the AMSR-E was developed and provided to the National Aeronautics and Space Administration's EOS Aqua satellite by the National Space Development Agency of Japan in 2002 [44]. The AMSR-E instrument has six microwave bands at 6.9–89 GHz,

TABLE I
SUMMARY OF MAJOR PERFORMANCE AND CHARACTERISTICS OF AMSR-E INSTRUMENT [43]

Parameters	Performance and Characteristics						
Central frequencies (GHz)	6.925	10.65	18.7	23.8	36.5	89.0A	89.0B
Bandwidth (MHz)	350	100	200	400	1000	3000	3000
Polarization	Horizontal and Vertical Polarization (H & V)						
NEAT (K)	< 0.34	< 0.70	< 0.70	< 0.60	< 0.70	< 1.20	< 1.40
Spatial resolution (km)	50		25		15		5
Dynamic range (K)	2.7 to 340						
Beam width (°)	2.20	1.50	0.80	0.92	0.42	0.19	0.18
IFOV (km)	43×75	29×51	16×27	18×32	8.2×14	3.7×6.5	3.5×5.9
Swath width (km)	1450						

which are all dual polarized (H and V). The MBT sensitivity of five shorter bands is greater than 1 K, which satisfies the requirement in this study, and the spatial resolution at the ground surface varies from approximately 50 km at 6.9 GHz to 5 km at 89 GHz. The orbit of Aqua is sun-synchronous with equator crossings at 1:30 pm and 1:30 am local solar time, respectively. For details of the AMSR-E characteristics, see Table I.

MBT data at night time (local 1:30 am), including frequencies at 6.9, 10.7, 18.7, and 36.5 GHz, which are all not resampled and with H&V polarization, were selected in this research to avoid the effects from solar radiation, and to make comparison on varied bands and on previous MBT results on Wenchuan earthquake. The data of 23.8 GHz was neglected because it locates at the peak of atmospheric vapor absorption, and the data of 89.0 GHz was also rejected for its poor temperature resolution and sensitivity to atmospheric water vapor [35]. Additionally, the time domain for this research ranges from 2003 to 2011 covering the entire observation period of AMSR-E.

The diameter of preparation zone of Mw7.9 Wenchuan main shock calculated from Dobrovolsky's equation [45] is 3000 km about, which is much larger than the swath width of AMSR-E data. It is hard for the whole preparation zone to be completely covered by a single swath. Thus, to ensure the valid coverage of retrieved MBT inside the selected area, a moderate geographical region (26°–36°N, 98°–108°E) approximately centered at the epicenter of Wenchuan earthquake on Longmenshan faults was selected in this study referring to both the size of earthquake preparation zone and the swath width of the AMSR-E data.

Meanwhile, because of the periodic orbit of the AMSR-E instrument, some part of the data covering the study area were occasionally missed, which leads to final retrievals being limited to incomplete region. Therefore, a slid-window process was conducted to fill the missed pixels with the average of data 14d before and 14d after the data-missing day, considering that there were little changes during this short-term period compared to the general variation trend of stable factors. Meanwhile, the sliding time window is identified as 28d in order to smooth the periodic effects of monthly celestial tidal stress on historical background, which may cause additional force on crustal stress as well potential impacts on seismic thermal anomaly in process of earthquake preparation [46].

$$T(x, y, t) = \frac{1}{2n} \sum_{i=t-n}^{t+n} T(x, y, i) \quad (n = 14) \quad (7)$$

where (x, y) is the geolocation of any pixel. t is the date of data-missing to be filled. n represents half the number of adjacent days. $T(x, y, i)$ is the observation data of any adjacent day i at (x, y) . $T(x, y, t)$ is the average MBT of adjacent 28d with all valid observation $T(x, y, i)$.

IV. RESULTS AND DISCUSSION

A. Comparison Between Two Methods

Based on the algorithms and methodology mentioned above, a carefully comparison was conducted with MBT data of H polarization at 18.7 GHz as an example, which was widely selected to detect microwave signals related to seismic activities [26]–[30], to analyze the differences of spatio-temporal evolution 5 days before and after the main shock (see Fig. 2) by using STW-TSM and the original TSM. Three indices were defined for making the comparison: 1) coverage index (CI) depicted as in (8), representing the calculation coverage, i.e., the ratio of the number of valid pixels to the total of the studied area; 2) normalized adjacency index (NAI) defined in (9), considering the georelationship between the epicenter and significant abnormal pixels; 3) entropy index (EI) calculated according to (10), which quantifies the degree of confusion in the retrieved cleaned MBT residuals. In this study, pixels with anomalous MBT greater than the average of all positive values plus twice their variance were identified as significant sites. Each integer interval from the minimum to the maximum of the range of cleaned MBT residuals falls into a class, i.e., from -6 K to 12 K in the following maps. Fig. 3 shows the detailed sequential results of these three indices 60 days (31 time slices) before and after the main shock.

$$CI = \frac{n_v}{N_m} \times 100\% \quad (8)$$

$$NAI = \frac{\sum_{i=1}^q \frac{v(x_i, y_i)}{(x_i - x_0) + (y_i - y_0)}}{q} \quad (9)$$

$$EI = - \sum_{i=1}^m p(i) \cdot \log_2 [p(i)] \quad (10)$$

where n_v refers to the number of pixels with valid MBT, while N_m stands for the total pixels inside the study region; q is the amount of significant anomaly points, (x_i, y_i) represents the geolocation of any significant anomalous pixel, $v(x_i, y_i)$ refers to the cleaned residual MBT value of point (x_i, y_i) , (x_0, y_0) is the geographic location of epicenter; m represents the total classes of

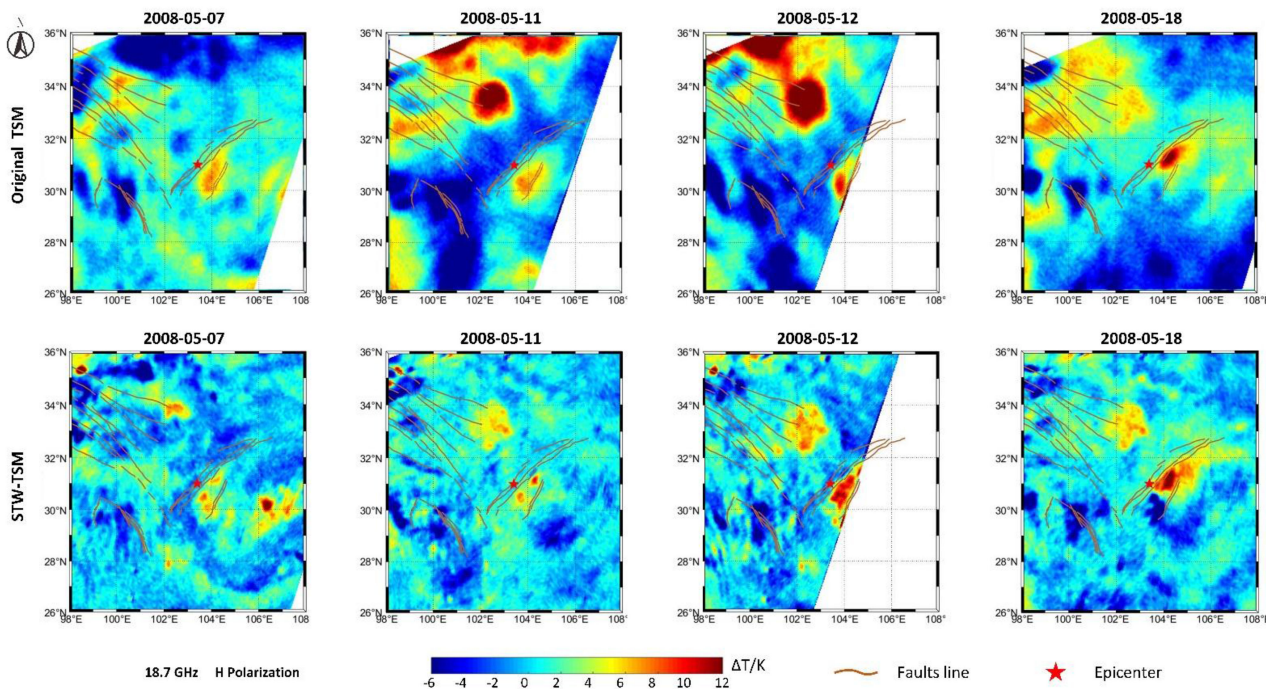


Fig. 2. Comparison of cleaned residual MBT of H polarization at 18.7 GHz from TSM (top) and STW-TSM (bottom).

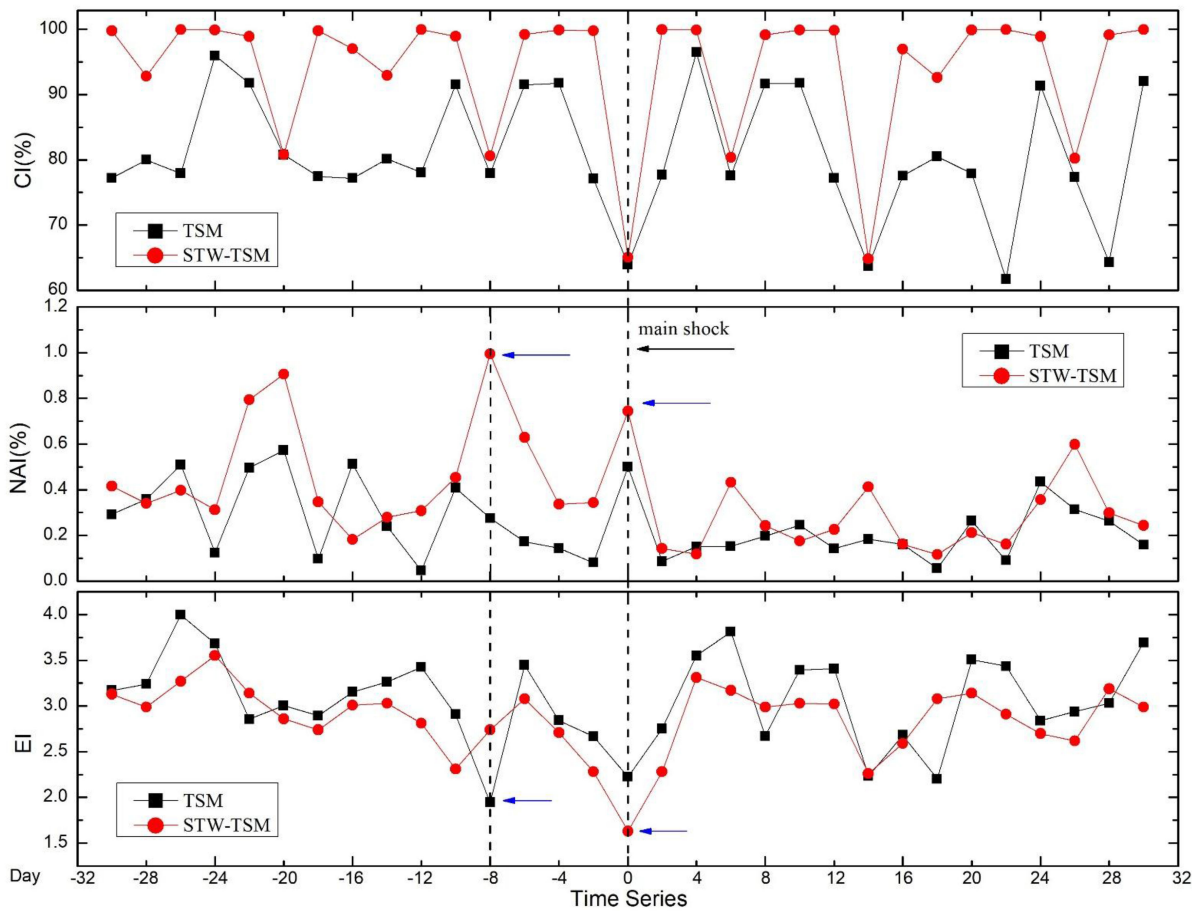


Fig. 3. Sequential results of three indices from the original TSM and STW-TSM. Time series consist of 31 historical time slices of MBT observations.

anomalous value range ($m = 18$ if cleaned MBT residuals range from -6 K to 12 K), while $p(i)$ is the probability of class i .

According to Fig. 2, there was significant anomalous MBT residuals appeared positively before and after the main shock, with clear differences in amplitude and spatial distribution of MBT residuals from TSM and STW-TSM. The positive MBT residuals from STW-TSM reveals more obvious strip-shaped anomalies close to the epicenter at the east of the Longmenshan faults, and the maximal MBT residual occurred on the main shocking day; while the positive MBT residuals from the original TSM did not show clearly this particular phenomenon. As for MBT residuals on May 11 and May 12 from the original TSM, large positive abnormal areas merged together, which means that nonearthquake disturbances (e.g., terrain) was not effectively removed. Besides, the STW-TSM could keep better coverage of the study area by slide-window operation overcoming the influence of satellite orbit somewhat, and richer information in detail inside the study area was uncovered. Noisy signals in the far-field of the study area were effectively suppressed by STW-TSM.

Fig. 3 shows the sequential results of CI, NAI, and EI from STW-TSM and TSM, respectively, in a time range with 60 days (31 time slices) before and after the main shock. First, the time series of CI revealed that the coverage ratio of cleaned MBT residuals from STW-TSM, after slide-window operation, is much higher than that from TSM. In addition, the sequence of NAI from STW-TSM was greater than that from TSM to varying degrees over the time domain except for seven time slices, and STW-TSM maintained relatively high NAI two weeks before the main shock. Moreover, the cleaned MBT residuals from STW-TSM showed a fluctuating NAI but with peak points on May 5 (NAI = 1.0) and May 12 (main shocking day, NAI = 0.8), which was superior to that from TSM. It indicates that the anomalous areas of cleaned MBT residuals from STW-TSM were revealed to be more relevant to the epicenter.

Furthermore, the entropy of retrieved maps represented a reliable measure of uncertainty and the degree of confusion in the range of cleaned residual MBT values, the anomalous areas could be better distinguished from normal regions if the entropy behaves low [47], and more obvious abnormal information possibly related to seismic activity might be uncovered. As shown in Fig. 3, the sequence of EI from STW-TSM were revealed at lower values than that from TSM with the proportion of 80.6% (25 time slices) over time, and the lowest point (as low as 1.7) was shown exactly on the main shocking day (May 12), while that from TSM was 8 days before (EI = 1.9). It means that STW-TSM are capable of showing greater heterogeneity in cleaned MBT residuals and better distinguishing the seismic-related abnormal areas in the retrieved MBT maps with normal regions.

According to above discussions, the performance of STW-TSM is much more satisfactory than TSM according to its general performances on all the three aspects (NAI, EI, and CI). So further analysis on MBT anomalies of Wenchuan earthquake sequence at different frequencies are based on the improved STW-TSM.

B. Comparison Between Two Polarizations

As claimed by Maki *et al.* [48], [49], microwave radiation energy generated by rock failures was detected at 300 MHz,

2 GHz, and 22 GHz in laboratory experiment, and 18.7 GHz was regarded more suitable for satellite sensors to detect earthquake-related MBT anomaly [19]–[21]. Additionally, decades of remote sensing rock mechanics experiments [50]–[56] have confirmed that there existed microwave radiation variation at many bands during rock deformation and fracturing, and different polarizations have diversified responses to the variation of rock stress. Nevertheless, most of previous studies [22], [23], [28]–[30] were conducted with MBT data at 18.7 GHz, which lack of fully investigation on multiple frequencies and dual polarization. Therefore, in this study, we investigated the MBT of H and V polarizations at multiple frequencies, aiming to compare the performance of H and V polarizations for better revealing seismic related MBT anomalies.

As shown in Fig. 4, although the uncovered positive anomalies of cleaned MBT residuals at H and V polarizations had similar spatial distribution, both the amplitude and the area of positive anomaly at H polarization were greater than that at V polarization, especially for the central abnormal strip east close to the epicenter. Singh *et al.* [24] found also the maximum rise in MBT at 37 GHz up to about 15 K was owing to horizontal polarization rather than vertical polarization. As for STW-TSM, we present that the maximal difference between the cleaned MBT residuals of H and V polarizations occurred at 6.9 GHz, and got week with frequency increases. For H and V polarizations at 36.5 GHz, the revealed positive anomalies of cleaned MBT residuals are much localized and behaved similar areas and amplitude.

C. Comparison Among Different Frequencies

According to Fig. 4, three positive anomalies of cleaned MBT residuals, one locates east close to the epicenter and two locate at the west of Longmenshan faults, uncovered at 6.9 GHz are very remarkable. The positive anomalies revealed at 10.7 GHz are much similar to that at 6.9 GHz, but a little strong for that east close to the epicenter and a little week for that to the west of Longmenshan faults. The positive anomalies uncovered at 18.7 GHz are similar to that at 10.7 GHz, but all the three ones are weaker than that at 10.7 GHz. The positive anomalies uncovered at 36.5 GHz are quite different from that at three lower frequencies.

The mechanism of above phenomena lies in that the microwave at high frequency has short wavelength and is sensitive to water vapor and small-scale meteorological disturbance due to its high spatial resolution. For high frequency, the satellite received seismic related microwave signals was mainly from very shallow subsurface, and it was easy to be polluted by water vapor and small-scale meteorological disturbances which cannot be thoroughly eliminated at the second step. While for low frequency, the satellite received seismic related microwave signals contain those from much deep subsurface, and it was relatively less polluted by atmospheric water vapor, and the small-scale meteorological disturbance could have been smoothed at rougher spatial resolution.

Furthermore, for cleaned MBT residuals of H polarization at different frequencies, Fig. 5 depicted the spatio-temporal evolution of positive MBT anomalies 10 days before and after the May 12 main shock. As for 6.9, 10.7, and 18.7 GHz, the

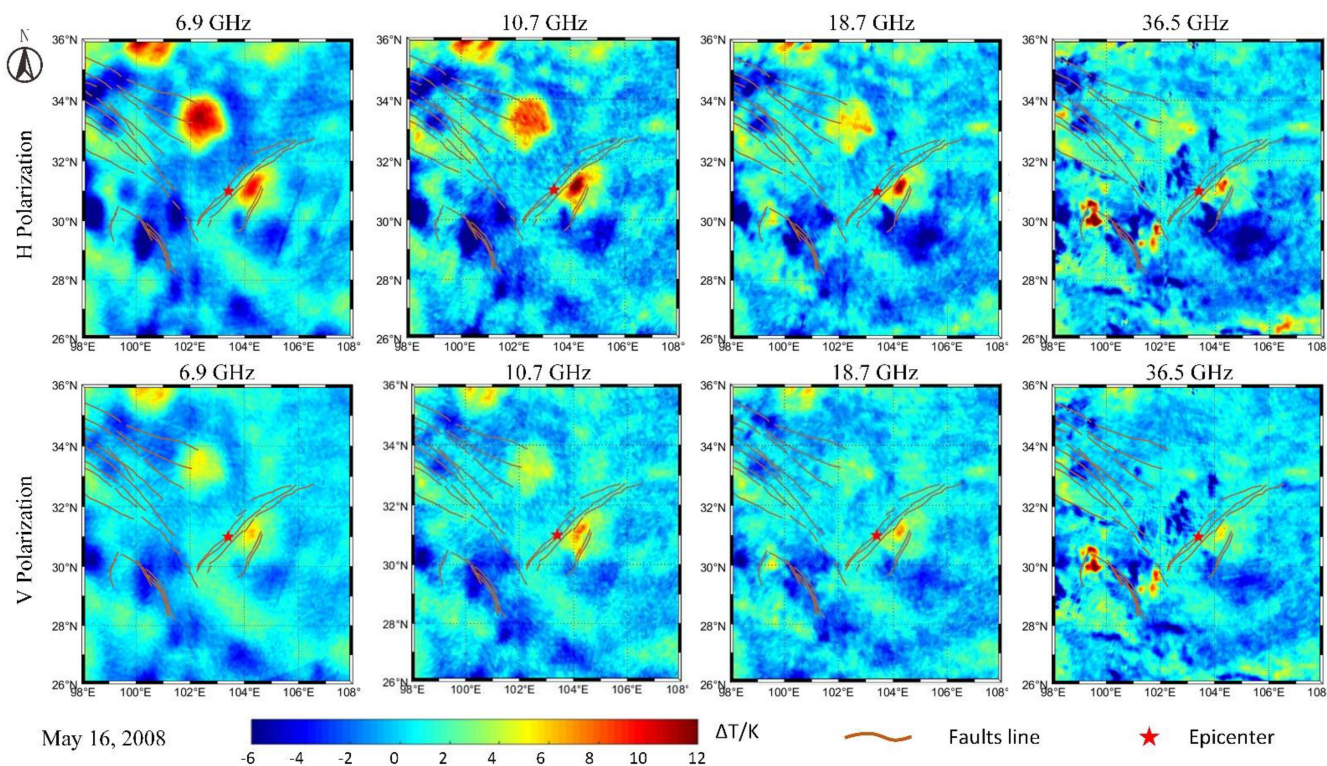


Fig. 4. Cleaned MBT residuals of H polarization (upper) and V polarization (lower) at different frequencies on May 16, 2008.

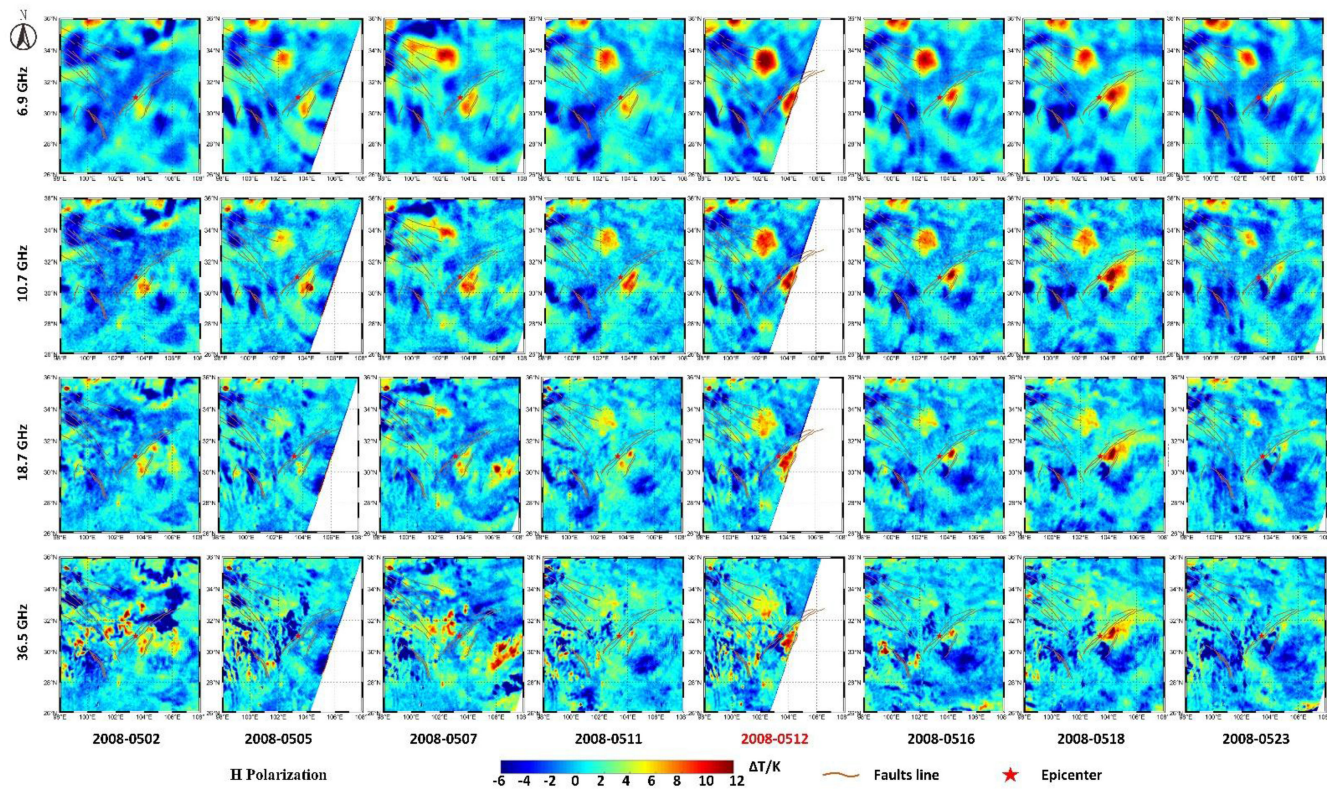


Fig. 5. Spatio-temporal evolution of cleaned MBT residuals of H polarization at different frequencies 10 days before and after May 12, Wenchuan earthquake.

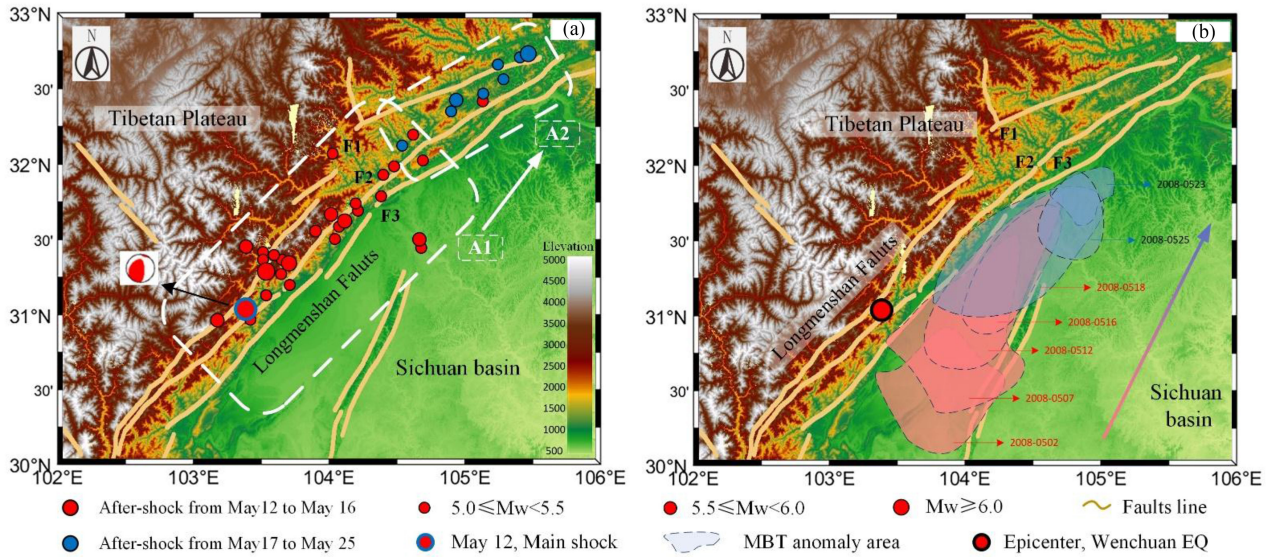


Fig. 6. Spatial distribution of after-shocks ($M_w > 5.0$, Depth < 30 km) and MBT anomaly areas (6.9 GHz) from the main shocking day to the end of May 2008. (a) Geolocations of after-shocks from May 12 to 16 gathered in area A1, and that from May 17 to 25 focused on area A2. (b) Central positive anomaly of MBT retrievals migrated northeastward with aftershocks.

central strip-shaped positive MBT anomaly first appeared on May 2 between Longmenshan faults and Longquanshan faults, where is a particular quaternary sedimentary zone. The abnormal areas became more and more significant until May 12. Then, the central strip-shaped positive MBT anomaly migrated along Longmenshan faults with aftershocks moving northeastward (see Fig. 6), and the abnormal areas dissipated subsequently by the end of May, 2008 with the disappearing of large aftershocks.

Ma *et al.* [28] reported positive anomaly of cleaned MBT residuals at 18.7 GHz on May 12, from the original TSM mainly, occurred at very local area east close to the epicenter. This anomaly was not so significant as that we got from STW-TSM. Maeda and Takano [19] revealed the most prominent abnormal pixels achieved the maximum of anomaly index at 18.7 GHz on May 13, 2008, 1d after the main shock, and gathered mostly at northwest along the Longmenshan faults. This anomaly is quasi-synchronous with the maximum anomalies of cleaned MBT residuals occurred on May 12, which revealed from STM-TSM as in Fig. 5. For what we got from the presented STW-TSM, it is worthy notice that 1) the central positive MBT anomalies at 18.7 GHz was relatively slight before the main shock, but much strong on the shocking day; 2) very localized positive MBT anomalies uncovered at 36.5 GHz had a wide distribution to the west of Longmenshan faults since May 2, but calmed down on May 11, 1 day before the main shock, which was in accordance with the general phenomena of “calm before a strong shock” [57]; 3) the general spatio-temporal evolution of positive MBT anomalies is similar to the geophysical pattern of earthquake preparation, shocking, and recurrence.

V. CONCLUSION

The first law of geography and its extension in time domain are applied to improve the algorithms involved in the two separated steps of TSM, and an improved TSM named STW-TSM was

developed. In the first step of STW-TSM, the historical time slices are given varied time-weights according to its time intervals with the shocking year, and a temporal weighting background is obtained to remove the general trend of MBT to retrieve basic MBT residuals; in the second step of STW-TSM, adjacent pixels inside a particular zone, referring to Dobrovolsky size and swath width, are endowed with varied space-weights according to its Euclidean distance away from the epicenter, and a spatial weighting reference basis is established to eliminate the regional meteorological noise remained in the basic MBT residuals, to retrieve cleaned MBT residuals related with seismic activities. With Wenchuan earthquake sequence in May, 2008 being a case, the application and effectiveness of STW-TSM are demonstrated. It is proved that nonseismic effects including terrain and meteorology can be removed effectively by STW-TSM, and more remarkable and better seismic-faults related seismic MBT anomalies can be uncovered by STW-TSM.

In this study, we discovered also that satellite MBT data at high frequencies presents some very localized positive MBT anomalies for its sensitive to water vapor and local meteorological noises, which need further validation with ground truth. The lower frequency bands with longer wavelength and stronger penetration ability could be less polluted by local meteorological noises, hence be more suitable for monitoring strong seismic activity and large earthquakes of broad preparation zone. While for possible MBT anomalies related with weak seismic activity and small-to-medium earthquake, it might be retrieved from microwave data at higher frequencies, if the noises from very local nonseismic effects can be effectively suppressed or identified.

Furthermore, if we can obtain a number of certain seismic concentration areas according to historical data and the known distribution of crustal faults, the future epicenters would be assumed to be distributed in some limited regions, so the STW-TSM can be further applied to real-time monitoring of seismic MBT anomalies for the certain focused areas.

However, some limitations remain in STW-TSM since the meteorological noises inside the study area varies with geolocation and terrain, which are difficult to be exactly simulated by spatial interpolation using limited far-field periphery points. If the MBT data observed by AMSR-E can be further corrected using quasi-synchronous observations from other satellite instruments carried on Aqua, the meteorological noises would be eliminated even more effectively, and the accuracy as well as the reliability of retrieved MBT residuals from STW-TSM could be greatly improved. Additionally, we were motivated by the results in this study, and more cases (e.g., the Iran–Iraq border earthquake sequence, Nepal earthquake sequence) are under careful processing to make further validation and improvement on the developed STW-TSM.

ACKNOWLEDGMENT

The authors' would like to thank the NASA's Earth Observing System Data and Information System for making AMSR-E images available to various research communities, and the editors and reviewers for their hard work on this article.

REFERENCES

- [1] V. I. Gornyi, A. G. Sal'Man, A. A. Tronin, and B. V. Shilin, "Outgoing infrared radiation of the earth as an indicator of seismic activity," *Dokl Akad Nauk SSSR*, vol. 301, pp. 67–69, 1988.
- [2] Z. J. Qiang, X. D. Xu, and C. G. Dian, "Case 27 thermal infrared anomaly precursor of impending earthquakes," *Pure Appl. Geophys.*, vol. 149, no. 1, pp. 159–171, 1997.
- [3] X. D. Xu, Z. J. Qiang, and C. G. Dian, "Thermal anomaly and temperature increase before impending earthquake," *Chin. Sci. Bull.*, vol. 6, pp. 291–294, 1991.
- [4] L. Piroddi and G. Ranieri, "Night thermal gradient: A new potential tool for earthquake precursors studies. An application to the seismic area of L'Aquila (central Italy)," *IEEE J. Sel. Topics Appl. Earth Observ. Remote Sens.*, vol. 5, no. 1, pp. 307–312, Feb. 2011.
- [5] A. A. Tronin, "Satellite thermal survey—A new tool for the study of seismoactive regions," *Int. J. Remote Sens.*, vol. 17, no. 8, pp. 1439–1455, 1996.
- [6] A. A. Tronin, M. Hayakawa, and O. A. Molchanov, "Thermal IR satellite data application for earthquake research in Japan and China," *J. Geodyn.*, vol. 33, no. 4–5, pp. 519–534, 2002.
- [7] D. Ouzounov and F. Freund, "Mid-infrared emission prior to strong earthquakes analyzed by remote sensing data," *Adv. Space Res.*, vol. 33, no. 3, pp. 268–273, 2004.
- [8] A. K. Saraf and S. Choudhury, "Satellite detects surface thermal anomalies associated with the Algerian earthquakes of May 2003," *Int. J. Remote Sens.*, vol. 26, no. 13, pp. 2705–2713, 2004.
- [9] A. K. Saraf and C. Swapnamita, "Thermal remote sensing technique in the study of pre-earthquake thermal anomalies," *J. Ind. Geophys.*, vol. 9, no. 3, pp. 197–207, 2005.
- [10] V. Tramutoli, V. Cuomob, C. Filizzola, N. Pergola, and C. Pietrapertosa, "Assessing the potential of thermal infrared satellite surveys for monitoring seismically active areas: The case of Kocaeli (Izmit) earthquake," *Remote Sens. Environ.*, vol. 96, no. 3–4, pp. 409–426, 2005.
- [11] L. X. Wu, S. J. Liu, and X. D. Xu, "Theoretical analysis to impending tectonic earthquake warning based on satellite infrared anomaly," in *Proc. Int. Geosci. Remote Sens. Symp.*, 2007, pp. 3723–3727.
- [12] L. X. Wu, K. Qin, and S. J. Liu, "GEOSS-based thermal parameters analysis for earthquake anomaly recognition," *Proc. IEEE*, vol. 100, no. 10, pp. 2891–2907, Oct. 2012.
- [13] A. Barkat *et al.*, "Thermal IR satellite data application for earthquake research in Pakistan," *J. Geodyn.*, vol. 16, pp. 13–22, 2018.
- [14] X. Z. Kong, N. Li, L. Lin, P. Xiong, and J. Qi, "Relationship of stress changes and anomalies in OLR data of the Wenchuan and Lushan earthquakes," *IEEE J. Sel. Topics Appl. Earth Observ. Remote Sens.*, vol. 11, no. 8, pp. 2966–2976, Aug. 2018.
- [15] C. Aliano *et al.*, "Robust TIR satellite techniques for monitoring earthquake active regions: Limits, main achievements and perspectives," *Ann. Geophys.*, vol. 51, no. 1, pp. 303–317, 2008.
- [16] M. Lisi *et al.*, "A study on the Abruzzo 6 April 2009 earthquake by applying the RST approach to 15 years of AVHRR TIR observations," *Natural Hazards Earth Syst. Sci.*, vol. 10, no. 2, pp. 395–406, 2010.
- [17] L. Piroddi, G. Ranieri, F. Freund, and A. Trogu, "Geology, tectonics and topography underlined by L'Aquila earthquake TIR precursors," *Geophys. J. Int.*, vol. 197, no. 3, pp. 1532–1536, 2014.
- [18] T. Maeda and T. Takano, "Discrimination of local and faint changes from satellite-borne microwave-radiometer data," *IEEE Trans. Geosci. Remote Sens.*, vol. 46, no. 9, pp. 2684–2691, Sep. 2008.
- [19] T. Maeda and T. Takano, "Detection of microwave signals associated with rock failures in an earthquake from satellite-borne microwave radiometer data," in *Proc. Int. Geosci. Remote Sens. Symp.*, 2009, pp. 61–64.
- [20] T. Takano and T. Maeda, "Experiment and theoretical study of earthquake detection capability by means of microwave passive sensors on a satellite," *IEEE Trans. Geosci. Remote Lett.*, vol. 6, no. 1, pp. 107–111, Jan. 2009.
- [21] T. Maeda and T. Takano, "Detection algorithm of earthquake-related rock failures from satellite-borne microwave radiometer data," *IEEE Trans. Geosci. Remote Sens.*, vol. 48, no. 4, pp. 1768–1776, Apr. 2010.
- [22] H. Chen and Y. Q. Jin, "A preliminary detection of anomalous radiation of rock failures related with Yushu earthquake by using satellite-borne microwave radiometers," *Remote Sens. Technol. Appl.*, vol. 25, no. 6, pp. 860–866, 2011.
- [23] B. Zhang, K. Qin, T. Wu, T. W. Shi, and W. Z. Fan, "Statistical analysis of microwave radiation anomaly before earthquake: A case study of Kamchatka Peninsula," *Acta Seismologica Sinica*, vol. 40, no. 1, pp. 98–107, 2018.
- [24] R. P. Singh *et al.*, "Recursory signals using satellite and ground data associated with the Wenchuan earthquake of 12 May 2008," *Int. J. Remote Sens.*, vol. 31, no. 13, pp. 3341–3354, 2010.
- [25] J. Yang and G. M. Guo, "Preliminary analysis of thermal anomalies before the 2010 Baja California M7.2 earthquake," *Atmosfera*, vol. 26, no. 4, pp. 473–477, 2013.
- [26] F. Jing, R. P. Singh, K. Sun, and X. H. Shen, "Passive microwave response associated with two main earthquakes in Tibetan Plateau, China," *Adv. Space Res.*, vol. 62, no. 7, pp. 1675–1689, 2018.
- [27] K. Qin, L. X. Wu, S. Zheng, and S. J. Liu, "A deviation-time-space-thermal (DTS-T) method for global earth observation system of systems (GEOSS)-based earthquake anomaly recognition: Criteria and quantify indices," *Remote Sens.*, vol. 5, no. 10, pp. 5143–5151, 2013.
- [28] Y. T. Ma, S. J. Liu, L. X. Wu, and Z. Y. Xu, "Two-step method to extract seismic microwave radiation anomaly: Case study of MS 8.0 Wenchuan earthquake," *Earthq. Sci.*, vol. 24, no. 6, pp. 577–582, 2011.
- [29] S. J. Liu, X. Liu, Y. T. Ma, and L. X. Wu, "Microwave radiation anomaly of Yushu earthquake and its mechanism," in *Proc. Int. Geosci. Remote Sens. Symp.*, 2012, pp. 1192–1195.
- [30] S. J. Liu, Y. T. Ma, and L. X. Wu, "Microwave radiation anomaly of wenchuan earthquake and its mechanism," in *Proc. Int. Geosci. Remote Sens. Symp.*, 2011, pp. 2500–2503.
- [31] L. X. Wu, C. Y. Cui, N. G. Geng, and J. Z. Wang, "Remote sensing rock mechanics (RSRM) and associated experimental studies," *Int. J. Rock Mech. Mining Sci.*, vol. 37, no. 6, pp. 879–888, 2000.
- [32] A. T. C. Chang, J. L. Foster, and A. Rango, "Utilization of surface cover composition to improve the microwave determination of snow water equivalent in a mountain basin," *Remote Sens.*, vol. 12, no. 11, pp. 2311–2319, 1991.
- [33] B. J. Choudhury, "Reflectivities of selected land surface types at 19 and 37 GHz from SSM/I observations," *Remote Sens. Environ.*, vol. 46, no. 1, pp. 1–17, 1993.
- [34] J. Cashion, V. Lakshmi, D. Bosch and T. J. Jackson, "Microwave remote sensing of soil moisture: Evaluation of the TRMM microwave imager (TMI) satellite for the Little River Watershed Tifton, Georgia," *J. Hydrol.*, vol. 307, no. 1–4, pp. 242–253, 2005.
- [35] F. T. Ulaby, R. K. Moore, and A. K. Fung, *Microwave Remote Sensing: Active and Passive. Volume 1-Microwave Remote Sensing Fundamentals and Radiometry*. Boston, MA, USA: Addison-Wesley, 1981, pp. 181–224.
- [36] W. R. Tobler, "A computer model simulating urban growth in the Detroit region," *Econ. Geograph.*, vol. 46, pp. 234–240, 1970.
- [37] H. J. Miller, "Tobler's first law and spatial analysis," *Ann. Assoc. Amer. Geograph.*, vol. 94, no. 2, pp. 284–289, 2004.
- [38] L. X. Wu and S. J. Liu, "Remote sensing rock mechanics and earthquake infrared anomalies," *Adv. Geosci. Remote Sens.*, vol. 34, pp. 710–741, 2009.

[39] S. A. Pulinets and K. A. Boyarchuk, *Ionospheric Precursors of Earthquakes*. Berlin, Germany: Springer, 2004, pp. 129–169.

[40] S. Pulinets and D. Ouzounov, “Lithosphere–atmosphere–ionosphere coupling (LAIC) model—an unified concept for earthquake precursors validation,” *J. Asian Earth Sci.*, vol. 41, pp. 1–382, 2011.

[41] Y. Bai *et al.*, “A geographically and temporally weighted regression model for ground-level PM_{2.5} estimation from satellite-derived 500 m resolution AOD,” *Remote Sens.*, vol. 8, no. 3, 2016, Art. no. 262.

[42] R. Saunders, M. Matricardi, and P. Brunel, “An improved fast radiative transfer model for assimilation of satellite radiance observations,” *Quart. J. Roy. Meteorol. Soc.*, vol. 125, no. 556, pp. 1407–1425, 1999.

[43] A. Singh, A. Yadav, and A. Rana, “K-means with three different distance metrics,” *Int. J. Comput. Appl.*, vol. 67, no. 10, pp. 13–17, 2013.

[44] T. Kawanishi *et al.*, “The advanced microwave scanning radiometer for the earth observing system (AMSR-E), NASDA’s contribution to the EOS for global energy and water cycle studies,” *IEEE Trans. Geosci. Remote Sens.*, vol. 41, no. 2, pp. 184–194, Feb. 2003.

[45] I. P. Dobrovolsky, S. I. Zubkov, and V. I. Miachkin, “Estimation of the size of earthquake preparation zones,” *Pure Appl. Geophys.*, vol. 117, no. 5, pp. 1025–1044, 1979.

[46] W. Y. Ma *et al.*, “Influences of multiple layers of air temperature differences on tidal forces and tectonic stress before, during and after the Jiujiang earthquake,” *Remote Sens. Environ.*, vol. 210, pp. 159–165, 2018.

[47] D. S. Angelo *et al.*, “Geosystemics view of earthquakes,” *Entropy*, vol. 21, no. 4, 2019, Art. no. 412.

[48] K. Maki, E. Soma, T. Takano, A. Fujiwara, and A. Yamori, “Dependence of microwave emissions from hypervelocity impacts on the target material,” *J. Appl. Phys.*, vol. 97, no. 10, 2005, Art. no. 104911.

[49] K. Maki, T. Takano, E. Soma, K. Ishii, and S. N. Yoshida, “An experimental study of microwave emissions from compression failure of rocks,” *J. Seismol. Soc. Jpn.*, vol. 58, no. 4, pp. 375–384, 2006.

[50] N. G. Geng, Z. F. Fan, Q. Q. Ji, C. Y. Cui, and M. D. Deng, “The application of microwave remote sensing technology in rock mechanics,” *Acta Seismologica Sinica*, vol. 8, no. 4, pp. 593–597, 1995.

[51] Z. F. Fan, Z. F. Fang, and M. D. Deng, “Basic experimental research of the microwave remote sensing applied in rock and soil engineering,” *Chin. J. Radio Sci.*, vol. 15, no. 4, pp. 410–414, 2000.

[52] Z. F. Fang *et al.*, “Application of passive microwave remote sensing technology to the seismic prediction and its physical mechanism,” *Chin. J. Geophys.*, vol. 43, no. 4, pp. 464–470, 2000.

[53] M. D. Deng, Z. F. Fan, Q. Q. Ji, C. Y. Cui, and N. G. Geng, “The experimental study for earthquake prediction by passive microwave remote sensing,” *J. Infrared Millimeter Waves*, vol. 14, no. 6, pp. 401–406, 1995.

[54] S. J. Liu, Z. Y. Xu, L. X. Wu, and B. Tang, “Theoretical analysis and experimental verification of microwave radiation features of fractured rock,” in *Proc. Photon. Electromagn. Res. Symp.*, 2014, pp. 1393–1400.

[55] S. J. Liu, Z. Y. Xu, J. L. Wei, J. W. Huang, and L. X. Wu, “Experimental study on microwave radiation from deforming and fracturing rock under loading outdoor,” *IEEE Trans. Geosci. Remote Sens.*, vol. 54, no. 9, pp. 5578–5587, Sep. 2016.

[56] Z. Y. Xu, S. J. Liu, and L. X. Wu, “Comparative study on the variation features of infrared and microwave radiation in deformation and fracture process of rock,” *J. Northeast. Univ.*, vol. 36, no. 12, pp. 1738–1742, 2015.

[57] M. Wyss and R. E. Habermann, “Precursory seismic quiescence,” *Pure Appl. Geophys.*, vol. 126, no. 2–4, pp. 319–332, 1988.



Yuan Qi received the B.S. degree from Northeastern University, Shenyang, China, in 2017. He is currently working toward the Ph.D. degree in photogrammetry and remote sensing with Central South University, Changsha, China.

His research interests include seismic thermal anomaly monitoring and geohazards perception and cognition.



Lixin Wu (Senior Member, IEEE) received the B.S. degree in mining survey from the China University of Mining and Technology, Xuzhou, China, in 1988, and the M.S. and Ph.D. degrees in geomatics from the China University of Mining and Technology, Beijing, China, in 1991 and 1997, respectively.

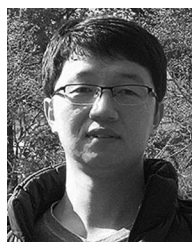
He is currently working with Central South University, Changsha, China, as a Leading Professor of geomatics with the School of geoscience and Info-physics.

Dr. Wu was the Co-Chair of User Applications in Remote Sensing Committee, IEEE Geoscience and Remote Sensing Society. He is currently a member of the Infrastructure Implementation Board of Group on Earth Observation, Chair of WG III-8 of ISPRS, member of China National Committee of ISDE, Vice Chairman of the Space Observation Committee of China Seismology Society, and Editor-in-Chief of the *Journal of Geography and Geo-Information Science* (Chinese).



Miao He received the B.S. degree from the Central South University of Forestry and Technology, Changsha, China, in 2016. She is currently working toward the M.Sc. degree in surveying and mapping engineering at Central South University, Changsha, China.

Her research interests include seismic aerosol anomaly monitoring and cognition.



Wenfei Mao received the B.S. and master’s degrees from Jilin University, Changchun, China, in 2011 and 2015, respectively. He is currently working toward the Ph.D. degree in digital mine engineering at Northeastern University, Shenyang, China.

His research interests include geohazards remote sensing and remote sensing rock mechanics.